DOI: 10.26599/FSHW.2026.9251064

Contents lists available at SciOpen

Food Science and Human Wellness

journal homepage: https://www.sciopen.com/journal/2097-0765

China Food Publishing Co.

Flammulina velutipes Polysaccharides Demonstrate an Impact on Metabolic Regulation via Gender-specific Modification of Key Gut Microbiota in Mice

Ruiqiu Zhao[a,b], Congcong Gao[a], Hongliang Yao[a], Hechao Du[a], Qiuhui Hu[c], Liyan Zhao[b,*]

[a] College of Animal Science and Food Engineering, Jinling Institute of Technology, Nanjing 210095, China

[b] College of Food Science and Technology, Nanjing Agricultural University, Nanjing 210095, China

[c] College of Food Science and Engineering, Nanjing University of Finance and Economics, Nanjing 210023, China

ABSTRACT: The objective of this study was to conduct a comprehensive evaluation of the transport characteristics, toxicological profiles, and functional physiological impacts of *Flammulina velutipes* polysaccharides (FVP), both *in vitro* and *in vivo*. Caco-2 cell model and murine model were employed to verify the objective in this paper, with a special emphasis on investigating gender-specific differences. The results revealed that FVP could traverse the Caco-2 cell monolayer via clathrin-dependent endocytosis. The acute oral toxicity assessment categorized FVP as minimally toxic. FVP administration led to a reduction in body weight, serum glucose and lipids levels on male and female mice, a mechanism attributed to the decreased gene expressions involved in glucose and lipids transporters in the intestinal tissue of mice. Moreover, FVP supplementation significantly influenced the levels of short-chain fatty acids and altered the abundance of pivotal gut microbiota, notably *P. goldsteinii* and *P. johnsonii* in male mice, and *B. sartoii* in female mice. PICRUSt analysis revealed enhanced functions in lipopolysaccharide biosynthesis, protein digestion and absorption in the intestine of male mice treated with FVP. Building upon our prior researches that underscored the multifaceted functional properties of FVP, this study further substantiates the functional characteristics of FVP in relation to glucose and lipid metabolism regulations.

Key Words: *Flammulina velutipes* polysaccharide, Transport characteristics, Glucose and lipid metabolism.

1. Introduction

The complex and dynamic interaction between gut microbiota and host's nutritional metabolism, significantly influences the initiation and progression of various metabolic disorders, encompassing metabolic syndrome [1], obesity [2], type II diabetes [3], non-alcoholic fatty liver disease [4], and other associated ailments. Consequently, alterations in gut microbiota composition have emerged as a promising new avenue for deciphering the mechanisms that underlie host physiological dysregulation. The composition and diversity of gut microbiota are altered by multiple factors, including but not limited to the host's age, dietary patterns, environmental exposures, and lifestyle choices. Upon mentioned above, dietary patterns stand out as the most modifiable and impactful determinant, with distinct microbial profiles observed in individuals adhering to Western diets (abundant in fats and proteins intake) compared to those following Eastern diets (abundant in

***Corresponding author**
zhlychen@njau.edu.cn

Received 6 October 2025
Received in revised from 14 November 2025
Accepted 8 December 2025

carbohydrates intake) [5]. As a result, researchers have increasingly directed their attention towards modulating gut microbiota through dietary interventions, such as integrating polysaccharide-rich [6] supplements to foster gut health.

Polysaccharides are natural high-molecular-weight compounds formed of over ten monosaccharide units, which are linked via glycosidic bonds to create either linear or branched structures. These biological macromolecules are widely distributed within the cell walls of plants and edible fungi. The unique bidirectional interactions between polysaccharides and gut microbiota, characterized by the targeted fermentation of polysaccharides by gut microbiota and the selective modulation of gut microbiota by polysaccharides, have garnered considerable interest due to their potential capacity to promote health or mitigate disease progression. Our prior studies isolated and explored a polysaccharide from *Flammulina velutipes* (designated as FVP), revealing its multiple functional attributes, including immune modulation [7, 8], anti-inflammatory effect [9], and lipid metabolism regulation both *in vivo* [10] and *in vitro* [11]. The functional properties of FVP have been thoroughly investigated, with its characteristics now relatively well-defined. Nevertheless, our comprehension of its toxicological profiles and transport mechanisms remains limited. Furthermore, existing functional studies predominantly relied on model animals or cell lines, resulting in a lack of systematic research concerning its fundamental physiological impacts on normal, healthy mice, particularly with the respect to gender-specific differences. As a step toward addressing this knowledge gap, the current study aims to investigate the absorption and transport characteristics of FVP across the Caco-2 cell monolayer *in vitro*. Additionally, the toxicological profiles, regulatory effect on intestinal metabolic functions as well as gut microbiota of FVP were evaluated in healthy male and female mice, taking into account of the gender-specific effects.

2. Materials and methods

2.1 Ethics statement

All animal procedures were conducted in strict accordance with the National Institutes of Health Guide for the Care and Use of Laboratory Animals (8th edition, 2011) as well as the Chinese National Standard GB/T 35892-2018 (Laboratory Animal Guideline for Ethical Review of Animal Welfare). The experimental protocol underwent thorough review and received approval from the Institutional Animal Care and Use Committee of Nanjing Agricultural University prior to study initiation.

2.2 FVP preparation, Caco-2 cells culture and cytotoxicity assay

The preparation and detailed characterization of FVP have been thoroughly documented in our previous studies [7]. To summarize, FVP was isolated from fresh *Flammulina velutipes* as a heteropolysaccharide (composed of mannose, glucose, xylose, arabinose and fucose). It consisted of two distinct components, with molecular weights measuring 7473.14 kDa (accounting for 48.09 %) and 15.077 kDa (accounting for 51.91 %), respectively.

Caco-2 cells (sourced from IBS Cell Experimental Center, Shanghai, China) were cultured in a complete culture medium (high-glucose Dulbecco's Modified Eagle Medium (DMEM) supplemented with 1% penicillin-streptomycin and 10% fetal bovine serum). The cells were incubated at 37 °C within a 5% CO_2 humidified incubator to maintain optimal growth conditions.

For the cytotoxicity assay, various concentrations of FVP solutions (0, 25, 50, 100, 200, 400 and 800 μg / mL) were prepared in DMEM. Caco-2 cells were seeded into 96-well plates at a density of 2×10^5 cells / mL and pre-cultured for 24 h. After this pre-culture period, the medium in each well was replaced with 100 μL of FVP-containing DMEM. The cells were then exposed to these FVP solutions for 48 h. Following the exposure period, 10 μL of Thiazolyl Blue Tetrazolium Bromide (MTT, 5 mg / mL) was added into each well and the incubation process was continued for an additional 4-hour. After that, the supernatant was carefully removed, and 200 μL of dimethyl sulfoxide (DMSO) was added into each well for 5 min. Finally, as an indicator of cell viability, the absorbance of the solution in each well was quantified at 570 nm using a plate reader (MQX200, BioTek Instruments, Inc., Vermont, USA).

2.3 Establishment and evaluation of the Caco-2 cells monolayer model

Following Shi's methodology [12], cells were seeded into Transwell plates (PET membrane with a diameter of 12 mm, an aperture of 0.4 μm, and an effective membrane area of 1.12 cm^2, Corning Incorporated, USA) at a density of 4×10^4 cells per chamber, with 0.5 mL of complete culture medium in apical chamber (AP side) and 1.5 mL in basolateral chamber (BL side). The medium was replaced every 48 hours during the initial 7-day period. Subsequently, the medium replacement frequency was increased to a daily basis. The cell monolayers were cultured for a total of 21 days to ensure complete differentiation.

The integrity of cell monolayers was evaluated through the followings. Firstly, transepithelial electrical resistance (TEER) values were measured with a Millicell ERS-2 volt-ohm meter. Secondly, alkaline phosphatase (AKP) activities were quantified via assay kit (Nanjing Jiancheng Bioengineering Institute, China) with AP ： BL activity ratio calculation. Finally, the permeability of the cell monolayers was assessed by measuring sodium fluorescein permeation. After rinsing the monolayers with Hanks balanced salt solution (HBSS), 0.5 mL of sodium fluorescein (400 μg / mL in HBSS) was added to the AP side, while 1.5 mL of HBSS was added to the BL side. At predetermined time points (30, 60, 90, 120, and 150 min), aliquots (200 μL) were sampled from the BL side with immediate HBSS replenishment to maintain volume consistency. The cumulative permeation of sodium fluorescein across the monolayer was determined from absorbance at 492 nm against a pre-established standard curve (the sodium fluorescein-HBSS curve).

2.4 Transportation of FVP in vitro

2.4.1 Bidirectional transport of FVP across Caco-2 cell monolayer

To establish a quantification curve (the FVP-HBSS curve) for subsequent analysis, standard solutions of FVP at varying concentrations were prepared in HBSS. The concentrations of FVP in these solutions were determined using the phenol-sulfuric acid spectrophotometric method at 490 nm. Prior to the transport studies,

pre-qualified Caco-2 cell monolayers were rinsed thrice with pre-warmed HBSS (37 °C), followed by a 30-min equilibration period in HBSS (0.5 mL in the AP side and 1.5 mL in the BL side).

For the AP-to-BL transport studies, 0.5 mL of FVP solution (200, 400, 800 μg / mL in HBSS) was filled to the AP side, while the BL side (acting as the receiving side) contained 1.5 mL of HBSS. Conversely, for the BL-to-AP transport studies, 1.5 mL of FVP solution (at the same concentrations as above) was filled in the BL side, with the AP side (now the receiving side) contained 0.5 mL of HBSS. At predetermined time points (30, 60, 90, and 120 min), 200 μL samples were collected from the receiving sides and immediately replaced with an equal volume of fresh HBSS. The concentration of FVP in the collected samples was then measured as described earlier, based on the FVP-HBSS curve, and the amounts of FVP transported across the cell monolayer at different time points were calculated and accumulated. To further quantify the transport efficiency, the apparent permeability coefficients (Papp) were calculated using the following formula:

$$Papp\ (cm / s) = (dQ / dt) / (A \times C_0) \quad (1)$$

Where dQ / dt represents the flux rate of FVP (μg / s), A is the effective membrane area (1.12 cm^2), C_0 is the rate of FVP from the donor to the acceptor compartment (μg / cm^3).

2.4.2 Uptake of FVP in Caco-2 cells

To quantify the uptake of FVP by Caco-2 cells, standard FVP solutions with different concentrations were prepared in ultrapure water, and a quantification curve (FVP-ultrapure water curve) was established using the identical method as delineated in Section 2.4.1.

Following the completion of the bidirectional transport experiments, the Caco-2 cell monolayers were rinsed thrice with pre-cooled HBSS (4 °C) to remove any extracellular FVP. The cells were then lysed by ultrasound in ultrapure water. After centrifugation, the supernatant was collected, and the concentration of FVP in the supernatant was measured. The amounts of FVP uptake by the cells were calculated based on the FVP-ultrapure water curve.

2.5 Animal feeding trials

The experimental animals were supplied from Nanjing Medical University (license number: SCXK<Jiangsu>2016-0002, Nanjing, China). All animal experiments were carried out at Nanjing Agricultural University (license number: SYXK<Jiangsu>2017-0007, Nanjing, China).

The mice were housed 5 per cage under controlled environmental conditions (25 ± 2 °C temperature, 55 ± 10 % humidity, 12 h light / dark cycle) with *ad libitum* access to diet (LAD3001M, formulated based on the AIN-93G diet, with detailed compositions and nutritional ingredients provided in **Table S1**) and water.

2.5.1 Acute oral toxicity assessment of FVP

The acute oral toxicity assessment of FVP was evaluated in specific pathogen-free (SPF) Kunming (KM) mice adhering to the guidelines outlined in the Chinese National Standard GB/T 21084. A total of forty 8-week-old mice (20 males, 26 ± 2 g, and 20 females, 24 ± 2 g) were acclimated for a 7-day period. The mice were then randomly allocated, by sex, into 4 groups. The FVPm group (n=10 males) received a gavage of 300

mg / kg FVP on the 1st day, followed by a 14-day observation period. For the surviving mice, a subsequent gavage of 2000 mg / kg FVP was administered on the15th day, with another 14-day observation period. The CONm group (*n*=10 males) served as the control and received a gavage of 0.9 % saline at a dose of 0.1 mL per 10 g of body weight. The FVPf group (*n*=10 females) and the CONf group (*n*=10 females) underwent identical dosing protocols as their male counterparts, with FVP and saline, respectively. Throughout the study, food and water consumption, as well as body weight were recorded every 4 days. On the 29th day, the mice were euthanized via CO_2 asphyxiation followed by cervical dislocation. Major organs (brain, heart, liver, spleen, lungs, and kidneys) were excised and weighed. The organ indices were calculated using the following formula:

Organ index (mg / g) = Organ weight (mg) / Final body weight (g) (2)

2.5.2 Functional properties assessment of FVP

Forty SPF KM mice (20 males and 20 females, 4-week-old, 18 ± 2 g) were acclimated for 7 days. The mice were then randomly divided by sex into 8 groups (*n*=5). For the males, the SDm group served as the control, receiving a gavage of 0.9% saline at a dose of 0.1 mL per 10 g of body weight. The FLm, FMm, and FHm groups were administered a gavage of FVP at doses of 200, 400, 800 mg / kg / day, respectively. This dosage regimen was based on our previous research [9, 10], where 400 mg / kg / day was identified as the medium dose in this study and accordingly, adjustments were made to include both low- and high-dose groups. The females (SDf, FLf, FMf, and FHf) underwent identical dosing protocols with FVP and saline as their male counterparts. The daily oral gavage was administered for 4 weeks. Food and water consumption, as well as body weight were recorded every 4 days. At the end of the experimental period, the mice were euthanized via CO_2 asphyxiation followed by cervical dislocation. Serum, intestinal tissues and contents (duodenum, jejunum, ileum, cecum, colon and rectum), and fecal samples were snap-frozen in liquid nitrogen and stored at -80 °C for further analysis. Serum glucose, triglycerides, and total cholesterol levels were quantified using enzymatic kits (Nanjing Jiancheng Bioengineering Institute, China) according to the manufacturer's protocols.

2.6 RNA extraction and qRT-PCR analysis

Based on our previous study [11], total RNA was extracted from various intestinal tissues (duodenum, jejunum, ileum, cecum, colon, and rectum) using TRIzol reagent (Vazyme Biotech Co., Ltd, Nanjing, China) following tissues homogenization. The purity and concentration of the extracted RNA were determined spectrophotometrically (NanoDrop 2000, Thermo Fisher Scientific Inc., USA). Subsequently, cDNA synthesis was carried out from 1 μg of the total RNA using HiScript III RT SuperMix (Vazyme Biotech) following the manufacturer's protocol.

For quantitative real-time PCR (qRT-PCR), reactions were set up in triplicate 20 μL reactions containing ChamQ Universal SYBR qPCR Master Mix (Vazyme Biotech) on a QuantStudio 6 Flex system (Thermo Fisher Scientific Inc.). The primer sequences for the targeted mouse genes were sourced from Sangon Biotech Co., Ltd. (Shanghai, China) and detailed in **Table S2**, including clathrin subunits (*Clta*, *Cltb*, and *Cltc*),

glucose transporters (*Slc2a1*, *Slc2a2*, and *Slc5a1*), cholesterol transporters (*Acat2* and *Npc1l1*), and long-chain fatty acids (LCFAs) transporter (*Slc27a4*). Glyceraldehyde-3-phosphate dehydrogenase (*Gapdh*) was used as the reference gene. The relative gene expression levels were calculated via the $2^{-\Delta\Delta Ct}$ method.

2.7 Short-chain fatty acids (SCFAs) contents determination

Drawing on our previous research [9], the standard acetic, propionic, *n*-butyric, *i*-butyric, *n*-valeric, 2-methylbutyric, and *i*-valeric acids were obtained from Standard Material Research and Development Center (China). The intestinal content samples (ileum, cecum, colon, and rectum, 100 mg each) were homogenized in 1 mL of ultrapure water, centrifuged (10000 rpm, 10 min, 4 °C) and filtered (0.22 μm nylon).

Gas chromatography (GC) analysis was conducted using an Agilent 8860 GC system (Agilent Technologies Inc., USA), equipped with a flame ionization detector (FID) and a DB-WAX capillary column (30 m × 0.25 mm × 0.25 μm). The operational parameters were set as follows, the injector temperature was 250°C with a split ratio of 19:1, the detector temperature was 250°C, helium was used as the carrier gas with a constant flow rate of 1.0 mL / min. The oven program commenced at 70 °C and was held for 1 min, then the temperature was increased at a rate of 15 °C / min to 160 °C and held for 6 min, then further increased at 30 °C / min to 210 °C and held for 3 min. For sample injection, 0.2 μL of the filtered supernatant was used.

2.8 16S rDNA sequencing

Fecal microbial DNA was extracted using the QIAamp Fast DNA Stool Mini Kit (Qiagen) following our established protocol [10]. DNA quality was assessed through 1% agarose gel electrophoresis and Spectrophotometry (NanoDrop 2000). The qualified samples were then processed by Genesky Biotechnologies Inc. (Shanghai, China). The V3-V4 hypervariable region of the bacterial 16S rRNA was targeted for amplification using primers 341F (5'-CCTACGGGNGGCWGCAG-3') and 806R (5'-GACTACHVGGGTATCTAATCC-3'). After amplification, the resulting libraries were sequenced on the NovaSeq 6000 platform, employing the SP-Xp (PE250) double-ended sequencing strategy. Following the sequencing step, bioinformatics analysis was conducted to decipher the microbial community and diversity.

2.9 Statistical analysis

The data in this study were presented as mean ± standard deviation. Statistical analyses were performed with ANOVA or T test using SPSS 22.0 (IBM Corporation, Armonk, NY). Data from different groups of independent trials were considered statistically significant and extremely significant when the *P*-value was < 0.05 and < 0.01. For gut microbiota analysis, the Wilcoxon rank sum test (two groups) or Kruskal–Wallis rank sum test (three or more groups) was employed. A multi-hypothesis test was performed on the *p* values using the Bonferroni method to evaluate significant difference in species diversity between groups. Spearman's correlation coefficients were calculated to assess correlations, and adjusted *p* values for the false detection rate were calculated by the Benjamini–Hochberg method.

3. Results and discussion

3.1 Transport characteristics of FVP in Caco-2 cell monolayer

The Caco-2 cell line, derived from human colonic adenocarcinoma, is widely employed in *in vitro* studies to simulate the intestinal environment for the investigation of drugs toxicity, transport and absorption mechanisms [12]. For the cytotoxicity assay, FVP exhibited no cytotoxic impact on Caco-2 cells within the dosage range of 25-800 μg / mL, as evidenced by the results of 48-hour MTT assay (**Fig. 1 A**). The formation of an intact Caco-2 cell monolayer was visually confirmed through the use an optical inverted microscope (×400) (depicted in **Fig. S1**) and further confirmed by assessing key monolayer integrity indicators. TEER values serve as a dependable indicator of the Caco-2 cell monolayers integrity and an average TEER value exceeding 350 Ω·cm² is indicative of a monolayer suitable for transport studies [13]. Specifically, the TEER values of the Caco-2 cell monolayers reached in 1009.49 ± 14.91 Ω·cm² on day 21 (**Fig. 1 B**). As a pivotal enzyme located in the brush border of intestinal epithelial cells, AKP acts as a marker for Caco-2 cell differentiation, the polarized AKP expression (AP ： BL > 2) signifies the maturation of brush border enzymes and as a characteristic feature of the small intestinal epithelium [14]. The AKP activity ratio (AP ： BL) was recorded at 2.07 on day 21, with AP side was recorded as 1.49 ± 0.09 and BL side was 0.72 ± 0.01 Gold's unit / 100 mL (**Fig. 1 C**). Furthermore, the Caco-2 cell monolayer exhibited a remarkably low level of fluorescein sodium permeation, with only 0.35 ± 0.06 μg detected at 30 min and a cumulative total of 2.41 ± 0.10 μg at 150 min, compared to the control chamber's 22.22 ± 0.02 μg (**Fig. 1 D**). Collectively, these results confirmed a functionally intact Caco-2 cell monolayer with validated barrier properties, enabling subsequent investigations.

The bidirectional transport of FVP across the Caco-2 cell monolayer over 120 min were illustrated in **Fig. 1 E** and **F**. Both the overall quantity of FVP transported from the AP to the BL side and vice versa exhibited a consistent upward trend throughout the 120-minute observation. Within the initial 90 min, the cumulative amount of FVP transported in the high-dose group (800 μg / mL) surpassed that of the medium- (400 μg / mL) and low-dose (200 μg / mL) groups in a time- and dose-dependent manner. While dietary carbohydrates are predominantly absorbed in the form of monosaccharides, recent research provided compelling evidence that certain polysaccharides can traverse the intestinal epithelia intactly. A polysaccharide derived from *Grifola frondosa* (with a molecular weight of 4130 kDa) demonstrated a time- and dose-dependent escalation in its transport volume across the Caco-2 cell monolayer [15]. As presented in **Fig. 1 G** and **H**, the Papp value of FVP during AP-to-BL transfer exhibited a decreasing trend with increasing dose and time. While from the BL to the AP side, only the Papp value of high-dose FVP demonstrated a negative correlation with time. Under identical dosage and time conditions, the Papp value of FVP transport from the AP to the BL side consistently exceeded than of the reverse direction. Artursson's research [16], which revealed that biomacromolecule with absorption rates ranging from 0 to 100 % in the human jejunum corresponded to Papp values between 5×10^{-8} to 5×10^{-5} cm / s during their transport across the Caco-2 cell monolayer, and, a Papp value over 1×10^{-6} cm / s signified effective absorption of the biomacromolecule. In our study, FVP consistently recorded Papp values above 1×10^{-6} cm / s during the transport process, indicating its effective absorption in the intestinal tract. **Fig. 1 I** illustrated the variations in the bidirectional transport rate of FVP at different concentrations. As the dose

escalated, the transport rates of FVP from the AP to the BL side were recorded as 19.83%, 12.88%, and 5.49%, respectively. In contrast, the rate from the BL to the AP side were significantly lower, at 3.19%, 1.82%, and 0.99%. Overall, FVP demonstrated a distinct preference for transport from the AP to the BL side over the reverse direction ($P < 0.05$), reflecting a greater absorption rate relative to its excretion rate when traversing the Caco-2 cell monolayer. **Fig. 1 J** and **K** depicted the total amount of FVP uptake and its rate by Caco-2 cells during the transport process. Within the increase of dosage, the total amount of FVP uptake demonstrated an upward trend, while the uptake rate decreased gradually. Under the identical dosage conditions, the uptake rate of FVP by cells from the AP to the BL side was greater than that from the reverse direction, highlighting the directional preference of FVP uptake by Caco-2 cells. Indeed, polysaccharides typically face difficulties in penetrating Caco-2 cells via passive diffusion, instead, they often utilize the transcellular transport pathway for cellular entry [17]. In light of these findings regarding FVP, the intestinal absorption mechanism was slated for further clarification in subsequent animal experiments.

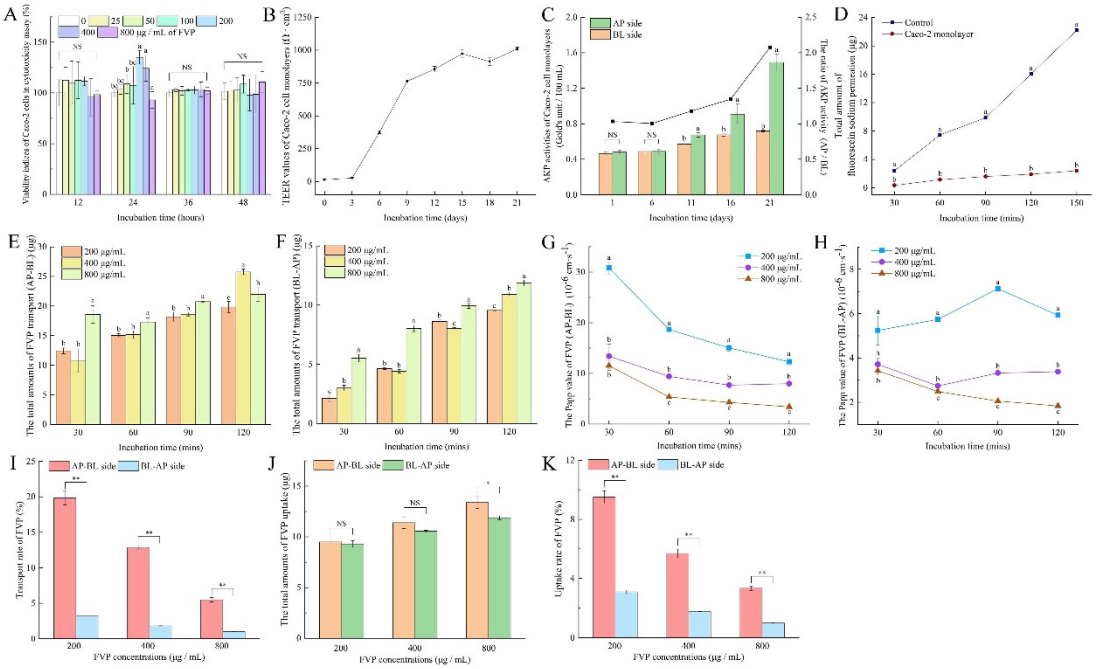

Fig. 1 Transport characteristics of FVP in Caco-2 cells monolayer (A-K): (A) The effects of FVP on Caco-2 cells proliferation index, (B) Trend of TEER value during Caco-2 cell monolayers formation, (C) AKP activities in AP and BL sides during Caco-2 cells monolayers formation, (D) Sodium fluorescein permeability of Caco-2 cells monolayers from AP to BL side, (E) The total amounts of FVP across Caco-2 cell monolayer from AP to BL side and (F) from BL to AP side, (G) The Papp values of FVP across Caco-2 cell monolayer from AP to BL side and (H) from BL to AP side, (I) The bidirectional transport rate of FVP across Caco-2 cell monolayer, (J) The total amounts of FVP uptake and (K) uptake rate in Caco-2 cells. Data were expressed as mean ± SD. different lowercase letters (a > b > c) indicated significant difference ($P < 0.05$) between different treatment groups in the same time point. * and ** indicated significant and extremely significant differences ($P < 0.05$ and $P < 0.01$) between different treatment groups in the same FVP dosage, NS indicated no significant difference.

3.2 Acute oral toxicity assessment of FVP in mice

During the 28-day toxicological assessment, the male and female mice in FVP treatment groups exhibited no mortalities or treatment-related adverse effects. All animals maintained normal clinical signs throughout this period, characterized by light pink skin free from scales, crusts, ulcers, redness or swelling; bright eyes without discharge; pink and clean auricles; and a moist nose. The FVP-treated mice exhibited coordinated gait and climbing activities, produced well-formed fecal pellets of uniform texture, and excreted

clear urine, all indicative of their good health and well-being. The body weight change curve (**Fig. 2 A)** indicated that both male and female mice in the FVP treatment groups experienced a slight, yet statistically insignificant, downward trend during the experimental period ($p > 0.05$). In toxicological studies, acute toxicity typically presents as abrupt weight loss, coupled with reduced food intake and activity levels [18]. In this study, the body weight gain, as well as feed and water consumption (**Fig. 2 B-D**) showed no significant differences between the FVP-treated groups and the controls both in males and females ($p > 0.05$). Organ indices are widely recognized as sensitive indicators of toxicological pathology [19]. Under normal physiological conditions, these indices remain within stable ranges, whereas toxicant-induced alterations can manifest as either an increase (suggestive of edema, congestion, hyperplasia, or hypertrophy) or a decrease (indicative of atrophy, degeneration, or necrosis) in the coefficient [20-23]. In our investigation, the stable organ indices (**Fig. 2 E**) indicated that FVP did not induce any significant pathological changes in the organs both in males and females, demonstrating the absence of hepatorenal toxicity, immunotoxicity, and neurotoxicity of FVP in rodent. In conclusion, FVP can be classified as a minimally toxic or practically non-toxic chemical, falling under category 5 of the Globally Harmonized System of Classification and Labeling of Chemicals (GHS), with an estimated LD_{50} ranging between 2000-5000 mg / kg, or potentially even lower actual hazard (for animal welfare considerations, toxicity test at a dose of 5000 mg / kg were not conducted in this research).

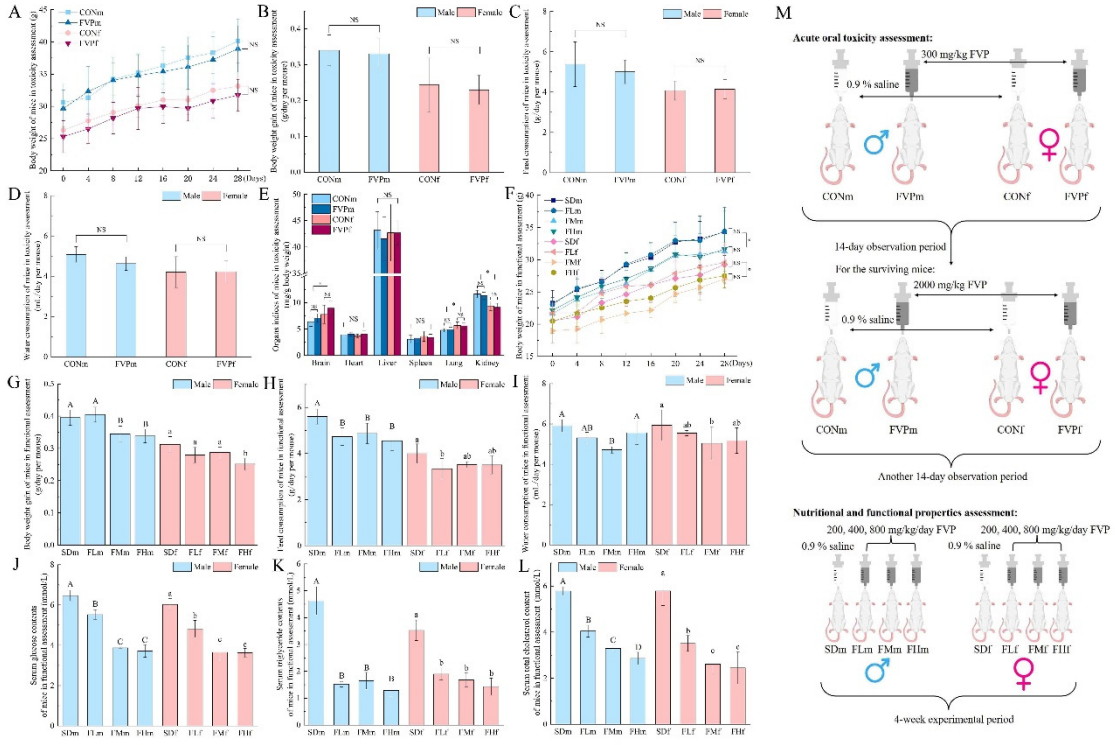

Fig. 2 Mice body profiles during FVP acute oral toxicity assessment (A-E): (A) Mice body weight changes, (B) Mice daily body weight gain, (C) Feed consumptions of mice in each group, (D) Water consumptions of mice in each group, (E) Organ indices of mice in each group. Mice body profiles during FVP nutritional and functional properties assessment (F-L): (F) Mice body weight changes, (G) Mice daily body weight gain, (H) Feed consumptions of mice in each group, (I) Water consumptions of mice in each group, (J) Serum glucose levels of mice in each group, (K) Serum triglyceride levels of mice in each group, (L) Serum total cholesterol levels of mice in each group. (M) The flowchart of animal experiments. Data were expressed as mean ± SD, n=5. * indicated significant differences ($P < 0.05$) between different treatment groups, NS indicated no significant difference, different capital letters (A > B > C > D) indicated significant difference ($P < 0.05$) of male mice among SDm, FLm, FMm and FHm groups, different lowercase letters (a > b > c) indicated significant difference ($P < 0.05$) of female mice among SDf, FLf, FMf and FHf groups.

3.3 Functional properties of FVP in mice

Throughout the 28-day functional assessment, the FVP administration elicited dose-dependent impacts on growth parameters (**Fig. 2 F-I**). The average daily weight gain in the FMm (0.35 g / day) and FHm (0.34 g / day) groups of males was significantly lower than that in the controls ($P < 0.05$). Among the female mice subjected to FVP gavage, the average daily weight gain was recorded at 0.28 g / day (FLf group), 0.29 g / day (FMf group), and 0.25 g / day (FHf group), with a significant difference observed in the FHf group compared to the controls ($P < 0.05$). Irrespective of gender, mice receiving high doses of FVP exhibited lower body weight and reduced weight gain. Compared with our previous research [9], we observed that healthy C57BL/6J male mice fed with the same semi-purified feed also experienced weight loss after 7 weeks of FVP gavage (at a dose of 400 mg / kg / day). The serum glucose levels in mice were depicted in **Fig.2 J**, with controls registered averages of 6.46 mmol / L (males) and 6.03 mmol / L (females), respectively. Notably, FVP-treated induced a significant reduction in serum glucose levels in both male and female mice compared to their respective controls ($P < 0.05$). Similarly, as depicted in **Fig. 2 K** and **L**, serum triglyceride and total cholesterol levels also exhibited significant reductions following FVP administration ($P < 0.05$) in males and females, exhibiting a clear dose-dependent manner. These findings are consistent with relative studies that have confirmed the serum glucose- and lipid-lowering properties of fungal polysaccharides. For instance, *Ganoderma lucidum* polysaccharides have been shown to modulate glucose metabolism through activating the AMPK pathway, led to a reduction in fasting blood glucose levels in type II diabetes model mice [24]. Additionally, *Auricularia auricula* polysaccharides were observed to significantly reduce both body weight and serum lipid levels in obese model mice induced by a high-fat diet, while reduced intestinal lipids transport [25]. In summary, these results collectively illustrated that FVP treatment effectively reduced both the serum glucose and lipids levels in mice of both sexes, highlighting its potential physiological regulatory effects on glucose and lipid metabolism.

3.4 Alterations in clathrin subunits gene expression in the intestine tissues of mice

Clathrin, a large soluble protein complex consisting of heavy and light chains, constitutes the foundational structural framework for receptor-mediated endocytosis. Specifically, the light chains of clathrin are encoded by *Clta* and *Cltb*, while the heavy chain is encoded by *Cltc*. The relative expression levels of *Clta*, *Cltb* and *Cltc* across distinct intestinal segments in male and female mice were illustrated in **Fig. 3**. Our findings indicated that FVP treatment significantly elevated the expression of these clathrin subunit genes in the intestinal tract of both sexes compared to their respective controls ($P < 0.05$). To be specific, following FVP administration, *Clta* expression was particularly elevated in the large intestinal segments (cecum, colon, and rectum), whereas *Cltb* expression elevated in the small intestinal segments (doudenum, jejunum, and ileum). Meanwhile, *Cltc* expression exhibited a consistent upward trend throughout the entire intestinal tract in both sexes.

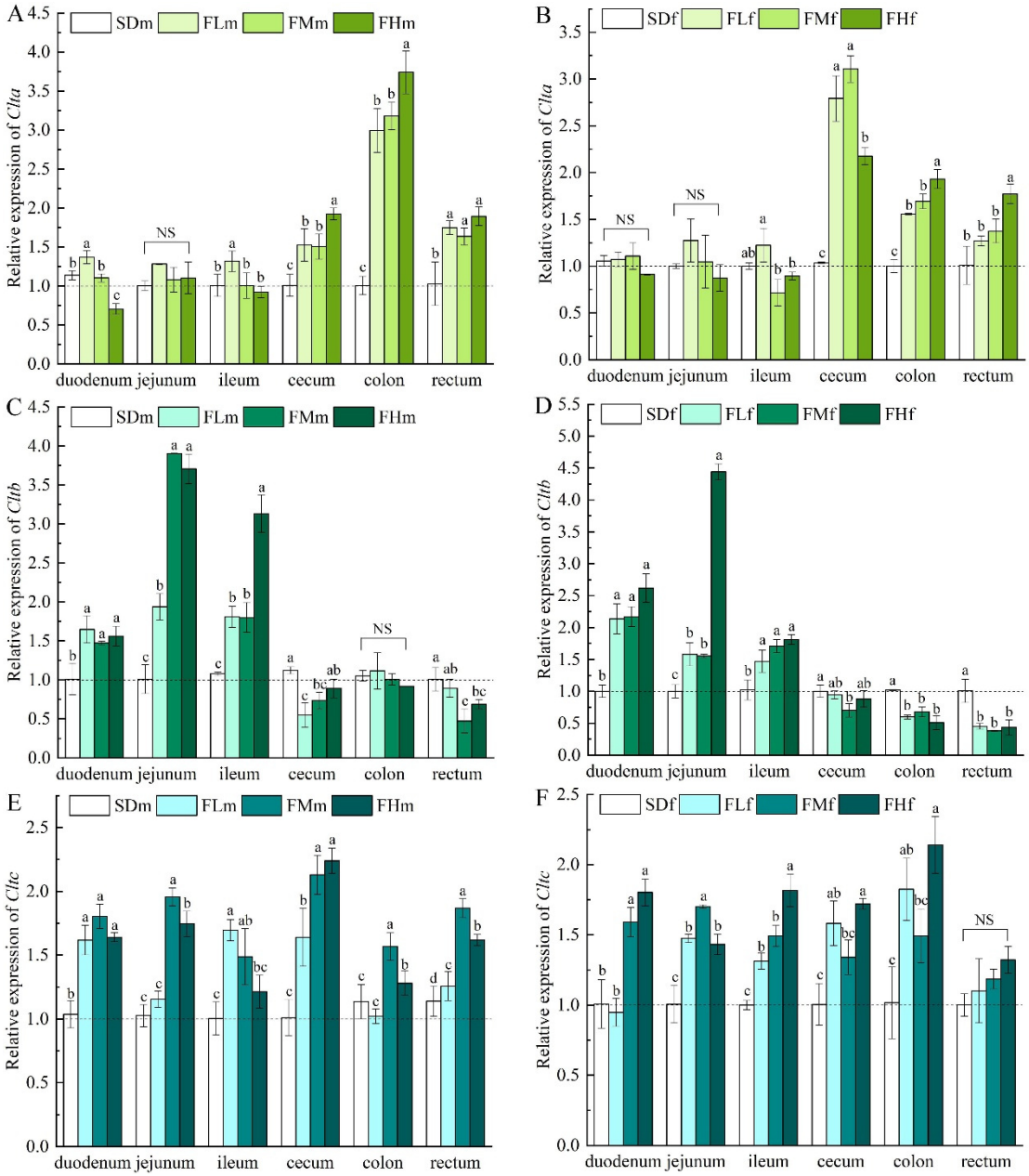

Fig. 3 The expressions changes of clathrin subunits genes including *Clta*, *Cltb* and *Cltc* in mice each intestinal segments tissues (duodenum, jejunum, ileum, cecum, colon and rectum) (A-F): *Clta* expressions in (A) male and (B) female mice intestinal segments tissues, *Cltb* expressions in (C) male and (D) female mice intestinal segments tissues, *Cltc* expressions in (E) male and (F) female mice intestinal segments tissues. Data were expressed as mean ± SD, n=5. Different lowercase letters (a > b > c > d) indicated significant difference ($P < 0.05$) between different treatment groups in the same intestinal segment, NS indicated no significant difference.

Biological macromolecules predominantly traverse the intestinal epithelium via transcellular (involves endocytic and exocytic processes) and paracellular pathways. Within intestinal epithelial cells, endocytosis can be broadly categorized into three principal pathways, clathrin-mediated endocytosis, caveolin-mediated endocytosis, and micropinocytosis [26]. Clathrin-mediated endocytosis, a classical pathway in animal cells facilitates nutrient uptake. This process commences with the initial interaction of extracellular macromolecules with the plasma membrane, triggering the assembly of clathrin molecules into polygonal lattice structures. These lattices, linked to their bound macromolecular cargo via the adaptor protein, ultimately facilitate the formation of clathrin-coated vesicle. The coated vesicle then pinches off from the

plasma membrane and moves into the cytoplasm for intracellular transport [27]. In contrast, caveolin-mediated endocytosis bind cholesterol and insert into the phospholipid bilayer of the plasma membrane through a characteristic hairpin conformation, thereby mediating macromolecule uptake [28]. Researchers have elucidated the endocytosis mechanisms of various polysaccharides in intestinal epithelial cells, revealing that both clathrin- and caveolin-dependent pathways regulate their absorption and transport [29, 30]. Relevant studies have also confirmed that FVP uptake *in vitro* occurs independently of the paracellular pathway [12]. Building upon established knowledge of FVP transport and uptake characteristics in Caco-2 cells and integrating findings from Section 3.1, this part further demonstrated that FVP transport is mediated by clathrin-dependent endocytosis.

3.5 Alterations in glucose transporter gene expression in the intestine tissues of mice

Cellular glucose metabolism relies on specialized glucose transporters, as glucose cannot passively traverse the lipid bilayer of the plasma membrane. These transporters, expressed in a wild range of tissues, can be broadly categorized into two distinct types, sodium-dependent glucose transporters (SGLTs) and facilitative glucose transporters (GLUTs). SGLTs utilize the sodium electrochemical gradient to actively transport glucose against its concentration gradient, while GLUTs facilitate glucose transport down its concentration gradient via facilitated diffusion. Among the various GLUT isoforms, GLUT1 and GLUT2 are predominantly expressed in liver, kidneys, and both the small and large intestines, GLUT3 and GLUT4 are mainly localized in testes and muscles [31]. It is well-documented that *Glut1*, *Glut2* (also known as *Slc2a1* and *Slc2a2*), and *Sglt1* (also known as *Slc5a1*) mediate D-glucose transport either via facilitative diffusion or sodium-dependent active transport, playing a pivotal role in intestinal glucose absorption [32]. **Fig. 4** illustrated the relative expression levels of genes associated with *Slc2a1*, *Slc2a2*, and *Slc5a1* across different intestinal segments in both male and female mice. Specifically, for *Slc2a1* (**Fig. 4 A** and **B**), the administration of medium or high doses of FVP significantly suppressed its expression in the jejunum, ileum and cecum of both sexes ($P < 0.05$). Conversely, FVP treatment upregulated *Slc2a1* expression in the colon of female mice, while in males, the increase was observed in the duodenum and rectum ($P < 0.05$). Similarly, *Slc2a2* expression was modulated by FVP (**Fig. 4 C** and **D)**. In females, *Slc2a2* expression was significantly downregulated in the jejunum, ileum, cecum, and rectum ($P < 0.05$). In males, significant decreases were observed in the ileum and cecum of the high-dose group ($P < 0.05$). As shown in **Fig. 4 E** and **F**, the regulatory effects of FVP on *Slc5a1* expression across intestinal segments was paralleled those on *Slc2a1*. FVP treatment significantly inhibited its expression in the jejunum, ileum and cecum of both sexes, while elevating it in the colon of females and the duodenum of males. Notably, these alterations mentioned above occurred without dose-dependent response. Relevant studies have indicated that the SGLT1 and GLUT2 are also involved in the cellular uptake of FVP [12], which explained the elevated expression of these transporters in the duodenum of both sexes. Overall, in the primary intestinal segments responsible for glucose absorption (jejunum and ileum), the expression of these two genes is actually downregulated following FVP treatment in both sexes. Given that the abundance and functional activity of these transporters directly determine cellular

glucose absorption capacity, our results suggested that FVP-treated leads to a marked reduction in dietary glucose absorption in these critical intestinal segments.

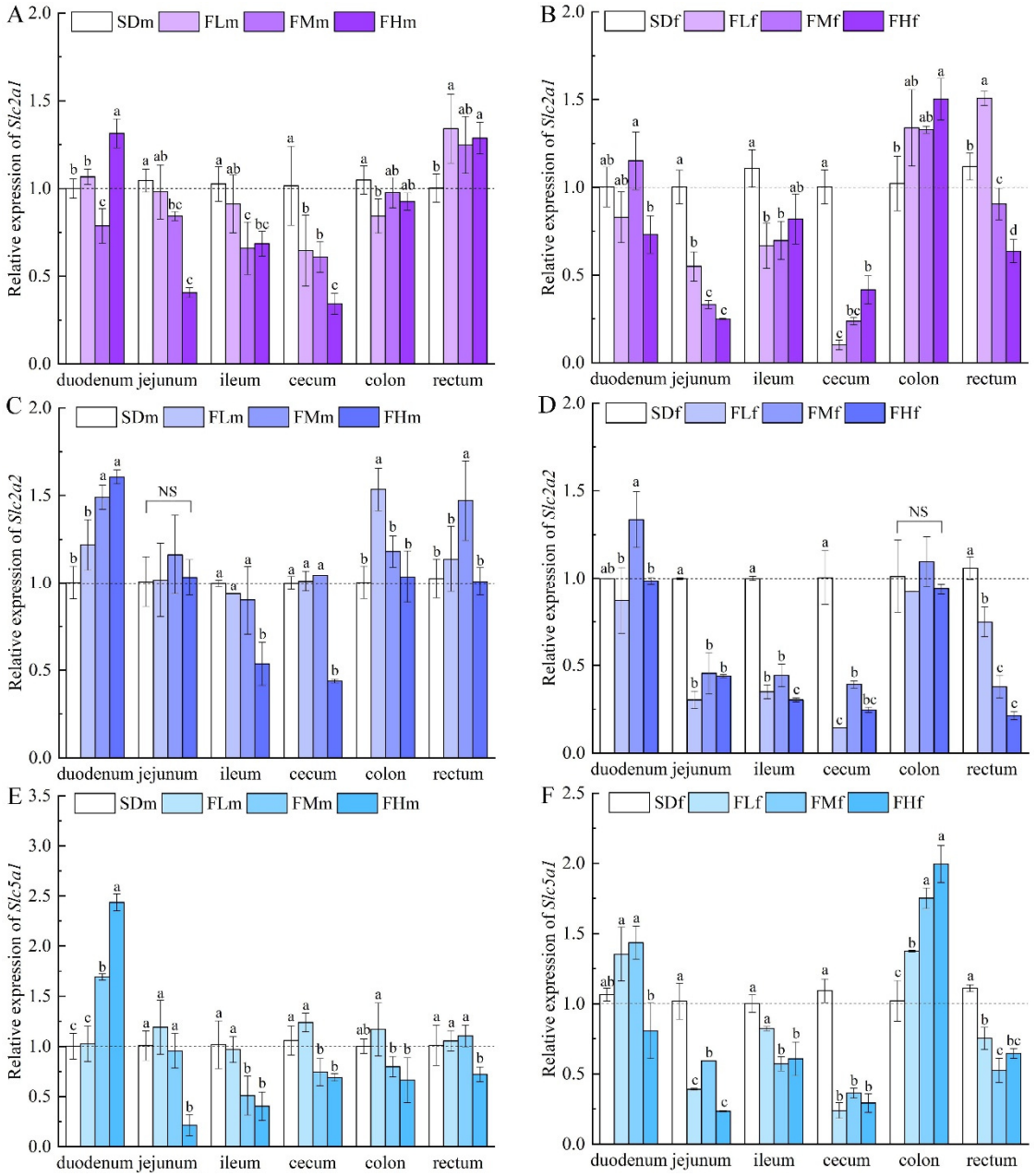

Fig. 4 The expressions changes of glucose transporter-related genes including *Slc2a1*, *Slc2a1* and *Slc5a1* in mice each intestinal segments tissues (duodenum, jejunum, ileum, cecum, colon and rectum) (A-F): *Slc2a1* expressions in (A) male and (B) female mice intestinal segments tissues, *Slc2a2* expressions in (C) male and (D) female mice intestinal segments tissues, *Slc5a1* in (E) male and (F) female mice intestinal segments tissues. Data were expressed as mean ± SD, n=5. Different lowercase letters (a > b > c > d) indicated significant difference (P < 0.05) between different treatment groups in the same intestinal segment, NS indicated no significant difference.

3.6 Alterations in lipids transporter gene expression in the intestine tissues of mice

The jejunum, situated in the middle section of the small intestine, represents the primary site for dietary cholesterol absorption, a process tightly regulated by intracellular cholesterol transporter NPC1L1 [33]. Acetyl-CoA acetyltransferase 2 (ACAT2) further contributes to cholesterol absorption by esterifying free cholesterol within enterocytes, thereby enhancing the absorption efficiency [34]. **Fig. 5 A-D** illustrated the relative expression patterns of cholesterol transporter-related genes (*Acat2* and *Npc1l1*) across distinct

intestinal segments in male and female mice. In females, FVP treatment induced marked downregulation of *Acat2* and *Npc1l1* in the jejunum, ileum, cecum and rectum, while conversely upregulating their expression in the colon ($P < 0.05$). In contrast, males exhibited decreased expression of both genes in the duodenum, jejunum, cecum, colon and rectum, with a selective upregulation observed solely in the ileum ($P < 0.05$).

In the proximal small intestine, fatty acid transporters (FATPs) play a pivotal role in facilitating the transport of LCFAs into enterocyte, which are subsequently incorporated into the triglyceride biosynthesis. Importantly, *Slc27a4* (also known as *Fatp4*) stands out as the sole FATPs expressed in the intestine, thereby serving as a crucial regulator of this absorptive process [35]. **Fig. 5 E-F** depicted the segmental expression patterns of *Slc27a4* across intestinal regions. The results revealed that FVP administration induced a notable reduction of *Slc27a4* expression within the jejunum and cecum of mice, while conversely upregulating its expression in the duodenum of both sexes ($P < 0.05$). Moreover, a gender-specific response was evident in the ileum and colon ($P < 0.05$). Particularly noteworthy is the consistent downregulation of *Npc1l1*, *Acat2*, and *Slc27a4* in the jejunum of both sexes following FVP gavage, which strongly implied a weakened transport function of cholesterol and LCFAs in this key intestinal segment.

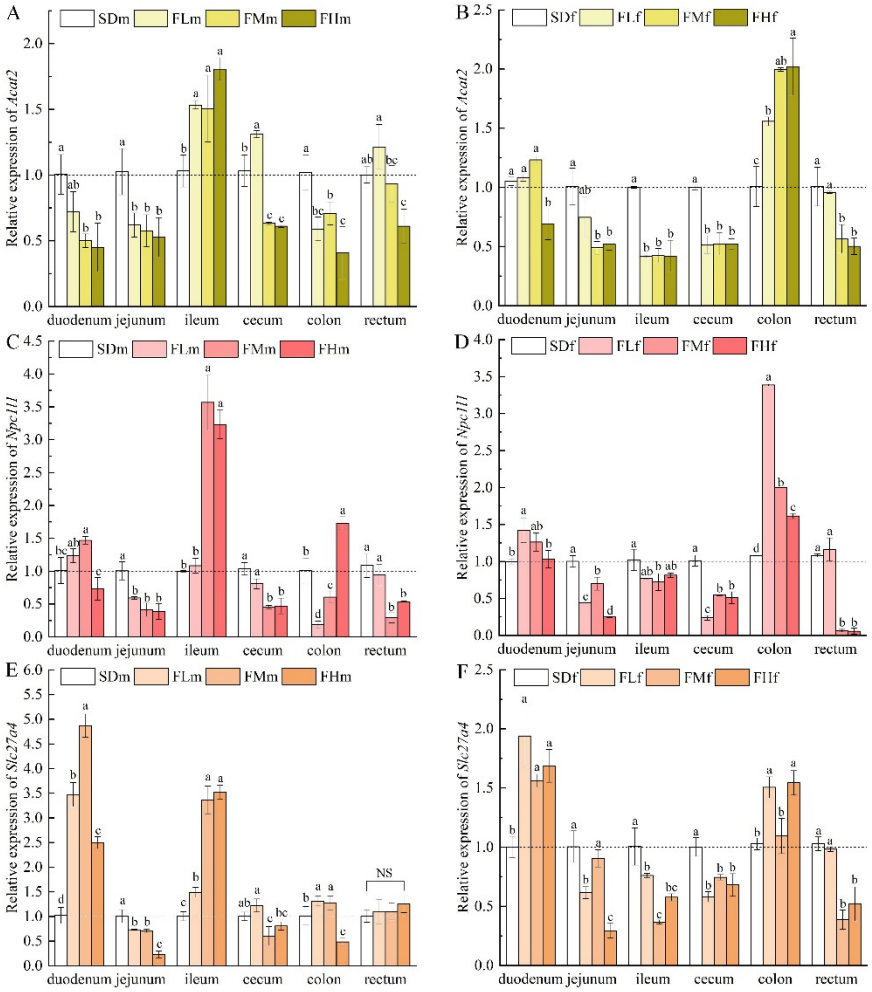

Fig. 5 The expressions changes of lipids transporter-related genes including *Acat2*, *Npc1l1* and *Slc27a4* in mice each intestinal segments tissues (duodenum, jejunum, ileum, cecum, colon and rectum) (A-F): *Acat2* expressions in (A) male and (B) female mice intestinal segments tissues, *Npc1l1* in (C) male and (D) female mice intestinal segments tissues, *Slc27a4* expressions in (E) male and (F) female mice intestinal segments tissues. Data were expressed as mean ± SD, n=5. Different lowercase letters (a > b > c > d) indicated significant difference ($P < 0.05$) between different treatment groups in the same intestinal segment, NS indicated no significant difference.

3.7 Alterations in SCFAs composition in the intestinal contents of mice

SCFAs are primarily produced through the microbial fermentation of dietary fiber by gut microbiota residing in the cecum and colon, with acetic, propionic and butyric acids constituting over 95% of the total SCFAs pool. Microbial metabolism also generates b-SCFAs, lactic acid, and succinic acid, although these minor metabolites occur in lower abundances, they still exert certain biological activities [36]. In absence of sufficient fermentable dietary fiber, gut microbiota utilizes dietary proteins that escape absorption in the small intestine or host-derived mucoproteins from the intestinal mucus layer, though their contribution to the overall SCFAs pool remains minimal, accounting for 17% in the proximal cecum and rising to 38% in the distal rectum [37]. Approximately 90-95% of the produced SCFAs are absorbed by the colonic epithelium and transported to the liver via the portal vein, with only 5-10% being exerted in feces [38]. In this research, the concentrations of SCFAs (including acetate, propionate, *n*-butyrate, and *n*-valerate acids) as well as branched short-chain fatty acids (b-SCFAs, including *i*-butyrate, *i*-valerate, and 2-methylbutyrate acids) across virous intestinal segments in mice were presented in **Fig. 6**. In the ileum, neither SCFAs nor b-SCFAs were detectable in the controls (SDm and SDf groups), whereas FVP administration induced dose-dependent increases of both SCFAs and b-SCFAs concentrations ($P < 0.05$). In the cecum, compared to the controls, there were dose-dependent elevations in the total and individual SCFAs (except for *n*-valerate and *i*-valerate acids) ($P < 0.05$ or $P < 0.01$). Interestingly, the total b-SCFA levels remained unchanged in females. In the colon, high-dose FVP administration significantly elevated the levels of both total and individual SCFAs and b-SCFAs in both sexes ($P < 0.05$ or $P < 0.01$), with similar trends observed in the rectal contents. Notably, the levels of propionate, *n*-valerate, *i*-butyrate, and *i*-valerate acids showed no significant changes in females but increased markedly in males ($P < 0.01$).

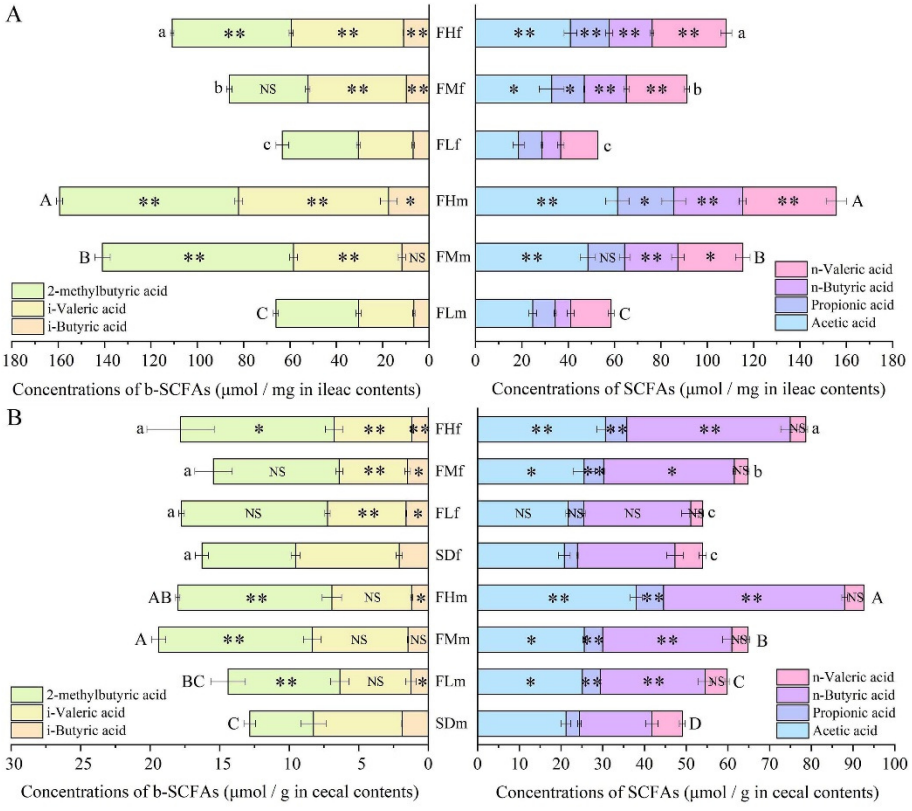

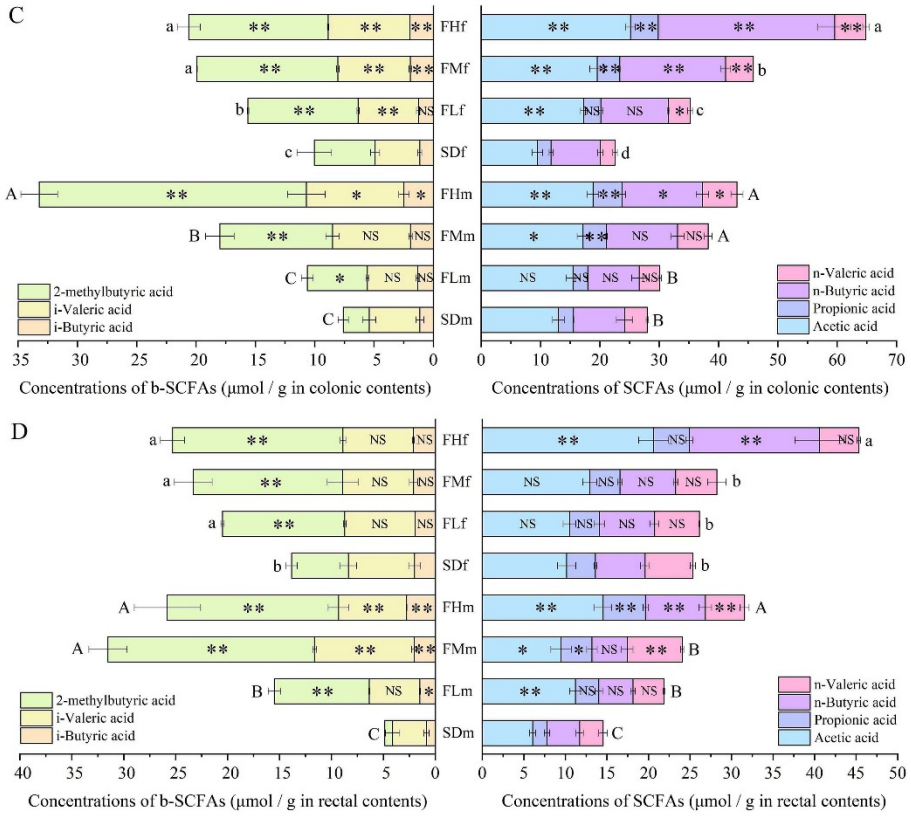

Fig. 6 Short chain fatty acids (SCFAs) and branched short chain fatty acids (b-SCFAs) concentrations in mice (A) ileum, (B) cecum, (C) colon, and (D) rectum. Data were expressed as mean ± SD, *n*=5. Different capital letters (A > B > C > D) indicated significant difference ($P < 0.05$) in total SCFAs or b-SCFAs concentrations of male mice among SDm, FLm, FMm and FHm groups, different lowercase letters (a > b > c) indicated significant difference ($P < 0.05$) in total SCFAs or b-SCFAs concentrations of female mice among SDf, FLf, FMf and FHf groups. NS, * and ** indicated no significant ($p > 0.05$), significant ($P < 0.05$) and extremely significant differences ($P < 0.01$) in individual SCFAs or b-SCFAs concentrations between FVP gavage groups with control (males and females were analyzed separately).

Extensive evidence has linked SCFAs to metabolic regulation, particularly in maintaining glucose and lipid homeostasis [39]. The conversion of acetate to acetyl-CoA in mitochondria consumes ATP, a process that could activate the AMPK signaling pathway [40]. Propionate and butyrate improve glucose homeostasis by modulating gut-derived hormonal signals and hepatic glucose production [41, 42]. Beyond these well-characterized SCFAs, b-SCFAs can mitigate insulin resistance through anti-inflammatory mechanisms or by improving mitochondrial function [43]. Our findings revealed that FVP administration led to dose-dependent increases in ileal SCFAs levels, suggesting enhanced polysaccharide fermentation in the small intestine. Moreover, FVP metabolism in the large intestine further promoted the individual SCFAs productions. Notably, in the controls, the concentrations of b-SCFAs in the distal large intestine remained low (less than 10 μmol / g of intestinal contents), but increased with FVP supplementation (the relative abundances of SCFAs and b-SCFAs were shown in **Fig. S2**). Overall, FVP fermentation enhanced the levels of SCFAs and b-SCFAs throughout the distal small intestine and the entire large intestines, while simultaneously modulating glucose and lipids metabolism pathways.

3.8 Regulatory effects of FVP on mice fecal microbiota

The structural changes of fecal microbiota were analyzed by the 16S rDNA sequencing and displayed in **Fig. 7** and **Fig. 8**, which showcase the relative abundances at the genus and species levels, respectively. For

reference, the relative abundance of major phyla, classes, orders, and families across different groups in fecal microbiota were presented in **Fig. S3**. In male mice (**Fig. 7 A-M**), dose-dependent increases were observed in the relative abundance of *Candidatus Arthromitus*, *Parabacteroides* and *Parasutterella* (**Fig. 7 C, E, J**). Specifically, **Fig. 8 A-C** further revealed species-level changes within the *Parabacteroides* genus in male mice. It was found that low and medium doses of FVP-treated enhance the relative abundance of *Parabacteroides johnsonii* (*P. johnsonii*) and *Parabacteroides goldsteinii* (*P. goldsteinii*), respectively. Notably, high-dose FVP gavage simultaneously elevated both species ($P < 0.05$). The gut-dwelling *Parabacteroides* genus plays pivotal roles in host-microbe co-metabolism, particularly in the high-fiber diets utilization. Equipped with extensive polysaccharide utilization loci, these bacteria degrade complex polysaccharides through specialized enzyme systems, gaining competitive advantages in fiber-rich environments [44]. Emerging evidence demonstrated their regulatory effects on host metabolism via indole derivatives (byproducts of tryptophan metabolism) and b-SCFAs, with significant implications for glucose and lipids homeostasis [45]. One study confirmed that the anti-obesity effects of *Hirsutella sinensis* polysaccharides were attributable to their prebiotic modulation of *P. goldsteinii* [46]. The enrichment of *P. goldsteinii* was correlated with increased level of intestinal ursodeoxycholic acid (UDCA) and reduced levels of taurine-conjugated bile acids through bile salt hydrolase (BSH) activity [47]. Another study revealed that *P. johnsonii* intervention mitigated colonic inflammation in mice with colon cancer by modulating the tryptophan metabolism pathway [48]. The relative abundance of *Parasutterella* were also found increased in males following FVP administration, although it lacks the capacity to degrade polysaccharide, it can modulate bile acid homeostasis and cholesterol metabolism through metabolite interactions [49].

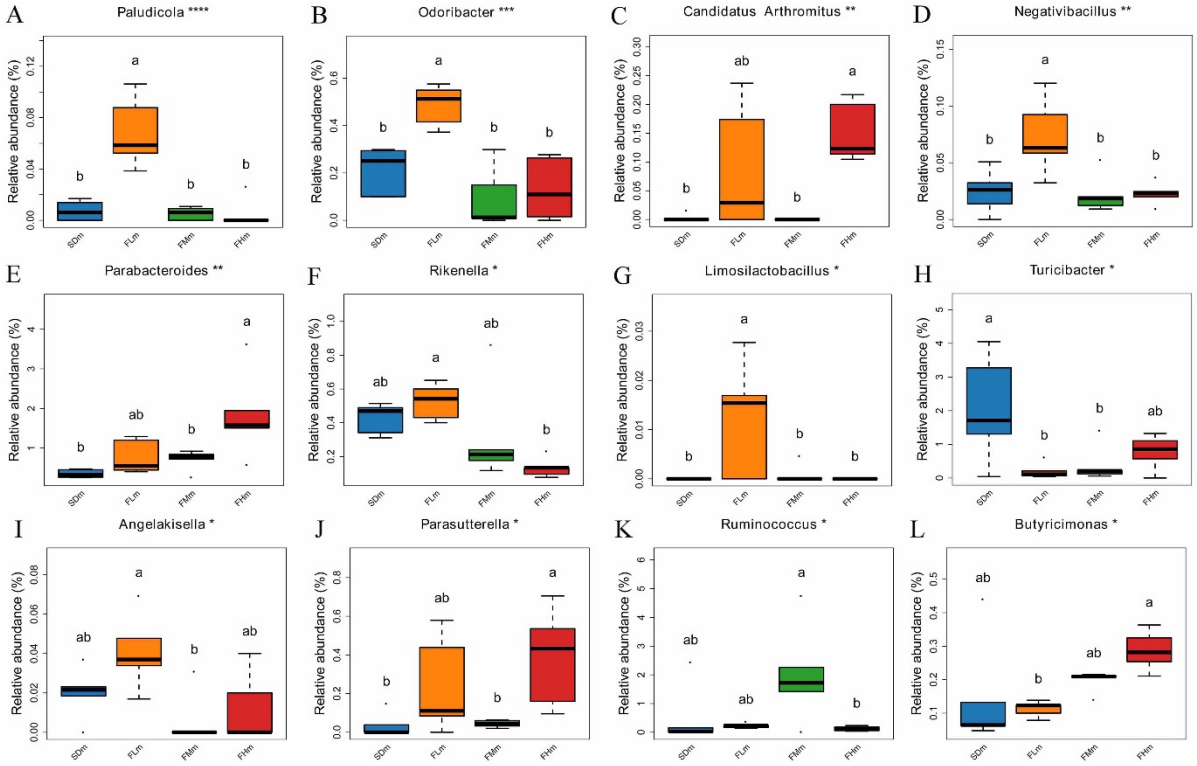

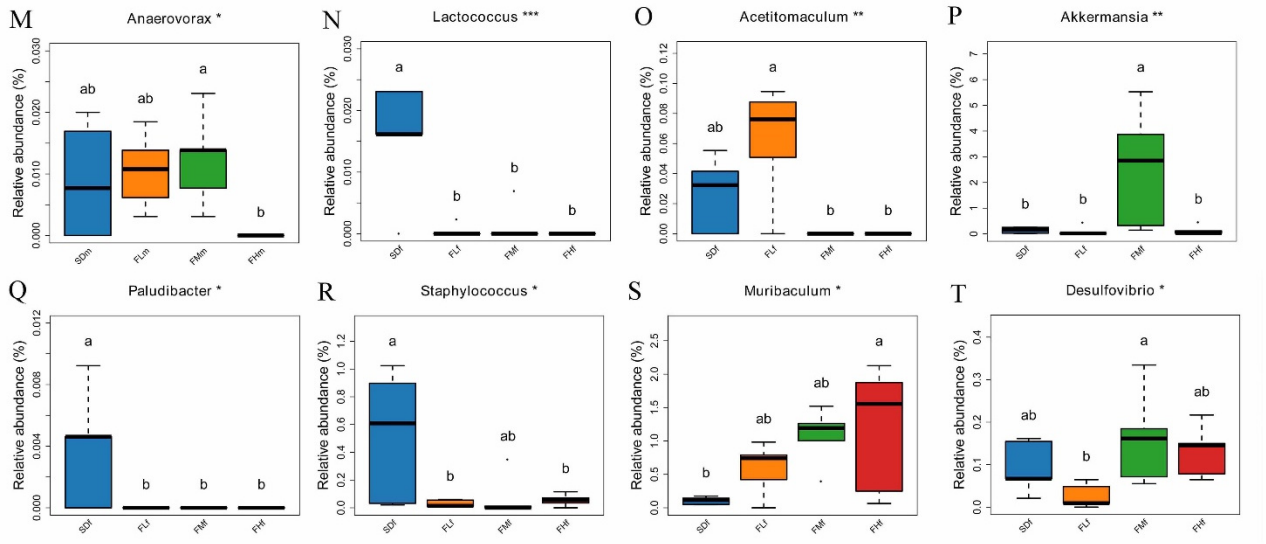

Fig. 7 Box plots of distinct bacterial composition in (A-M) male mice and (N-T) female mice feces at genus level. Data were expressed as mean ± SD, n=5. The * ($0.01 < P < 0.05$), ** ($0.001 < P < 0.01$), *** ($0.0001 < P < 0.001$) and **** ($P < 0.0001$) following the species names indicated p value size. Different lowercase letters (a > b > c > d) indicated significant difference between different treatment groups.

As illustrated in **Fig. 7 N-T**, unlike to the effects seen in males, female mice exhibited dose-dependent reductions in the abundances of *Lactococcus*, *Paludibacter*, and *Staphylococcus*, while the abundance of *Muribaculum* increased significantly. The notable reduction in the opportunistic pathogens *Lactococcus* and *Staphylococcus* created a healthier intestinal environment, as evidenced by the observation of reduced inflammation in mice fed a high-fat diet [50, 51]. Furthermore, restoring the *Muribaculum* through fecal microbiota transplantation counteracts the succinate accumulation induced by dietary fiber deficiency. This, in turn, promotes propionate production and enhances the intestinal anti-infective capacity [52]. Similarly, fucoidan-mediated *Muribaculum* enrichment improved bile acids homeostasis and alleviated ulcerative colitis symptoms in mice [53]. Delving deeper into species-level analysis in females (**Fig. 8 D** and **E**), we observed a decrease in the abundance of *Mucispirillum schaedleri* (*M. schaedleri*) in the FLf and FHf groups. Conversely, two *Bacteroides* species, *B. caecimuris* and *B. satroii*, exhibited increased abundances ($P < 0.05$). *M. schaedleri*, a low-abundance symbiotic bacterium residing in the intestinal mucosa, competes with *Salmonella* for anaerobic respiration substrates, thereby inhibiting the expression of *Salmonella* virulence factors and providing resistance against colitis [54]. However, its excessive accumulation can induce Crohn's disease-like pathology [55]. Hence, maintaining a low-abundance state of *M. schaedleri* is beneficial for strengthening anti-infection and anti-inflammatory responses in mice intestine. Studies on the intestinal microbiota of obese [56] and aging [57] mice have uncovered a significant reduction in the abundance of *P. goldsteinii*, as well as separately in *B. satroii* and *B. caecimuris*. These microbial alterations, particularly the notable reduction in abundance, compromised the intestinal defense system and impaired metabolic functions.

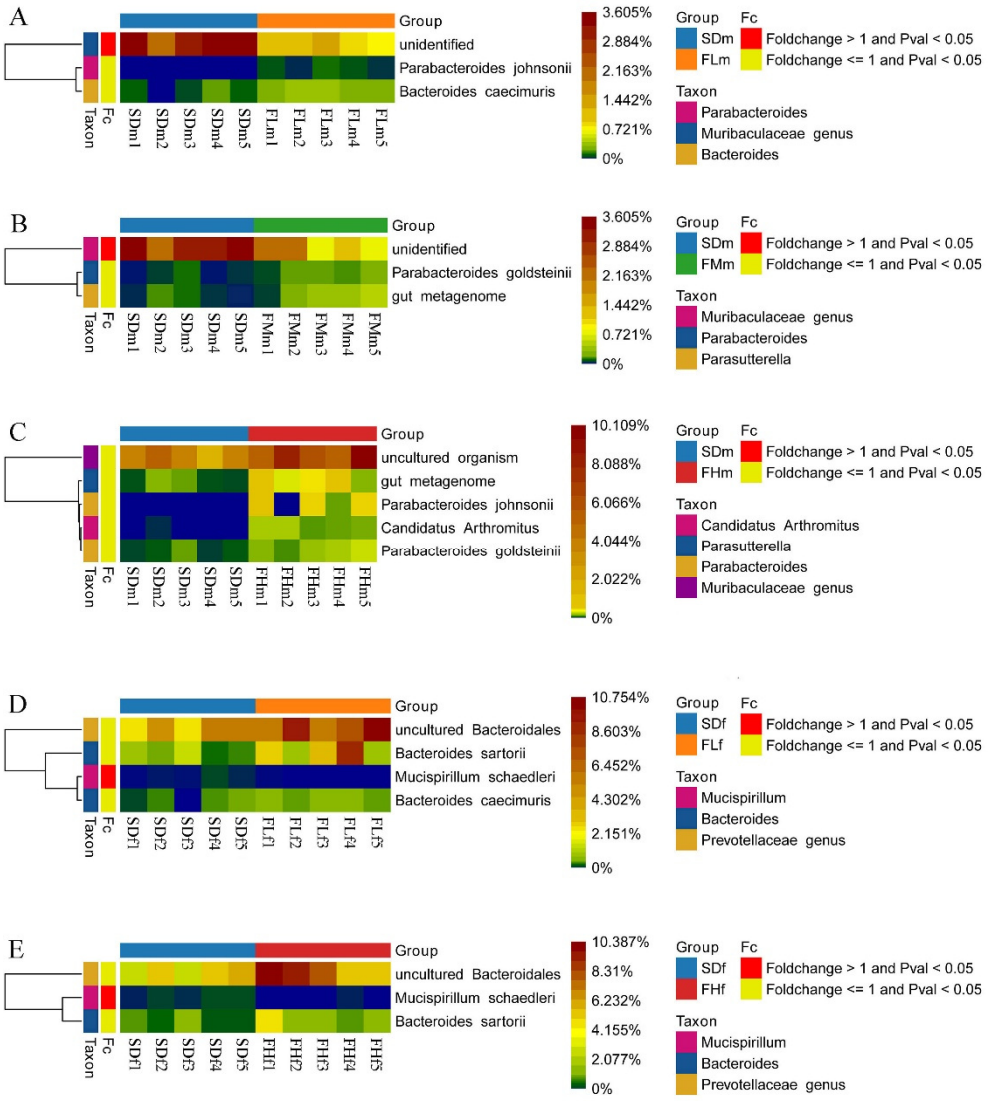

Fig. 8 Heatmaps of distinct bacterial composition in male and female mice feces at species level: (A) SDm vs FLm, (B) SDm vs FMm, (C) SDm vs FHm, (D) SDf vs FLf, (E) SDf vs FHf.

3.9 Correlation analysis in gut microbiota with rectal SCFAs contents and metabolic outcomes of mice

Fig. 9 A and **B** illustrated the results of Spearman correlation analyses that examining the associations between gut bacteria and rectal SCFAs profiles in male and female mice, respectively. Based on our genus- and species-level microbiota analyses (as shown in **Fig. 7** and **8**), we specifically selected 9 key taxa for this in-depth investigation. In male mice, the FVP-induced reductions in the abundance of *Lactococcus* and *Staphylococcus* demonstrated to be negatively correlated with the levels of propionic, *i*-butyric, *i*-valeric, 2-methylbutyric, and *n*-valeric acids. Conversely, polysaccharide-utilizing taxa including *P. goldsteinii* and *P. johnsonii* exhibited positive correlations with acetic, propionic, and *i*-butyric acids. Notably, *P. goldsteinii* also showed additional positive association with *i*-valeric, 2-methylbutyric, and *n*-valeric acids. In contrast, female mice exhibited positive correlations between *Muribaculum* and acetic, *n*-butyric, 2-methylbutyric acids, while *M. schaedleri* displayed inverse correlations with *n*-valeric acid. *Parasutterella* demonstrated male-specific positive associations with acetic, propionic, and butyric acids, with no such correlations observed in females. Moreover, the female-enriched genus *Bacteroides* demonstrated no correlations with any SCFAs or b-SCFAs, indicating its limited involvement in SCFAs and b-SCFAs metabolism pathways.

Fig. 9 Correlation analysis between mice gut microbiota and rectal SCFAs content (A-B): (A) male mice, (B) female mice. Correlation analysis between mice gut microbiota and metabolic outcomes (C-D): (C) male mice, (D) female mice. The *p*-value were adjusted by Benjamini-Hochberg method. * and ** indicated significant ($P < 0.05$) and extremely significant ($P < 0.01$) of the associations.

Fig. 9 C-D presented the results in examining the associations between gut bacteria and key metabolic parameters, including serum glucose and lipids levels, as well as jejunal expression of glucose or lipid transporter genes. In males, the FVP-induced alterations in *Lactococcus* were positively correlated with serum glucose and lipids levels. Conversely, *P. goldsteinii* and *P. johnsonii* exhibited inverse relationships with these metabolic markers. Moreover, *P. johnsonii* showed additional negative correlations with the jejunal expression of glucose transporters *Slc2a1* and *Slc5a1*, as well as lipids transporters *Npc1l1* and *Slc27a4*, suggesting broad inhibitory effects on intestinal nutrient absorption. *P. goldsteinii* selectively modulated lipid absorption pathways, showing negative correlations exclusively with *Acat2*, *Npc1l1*, and *Slc27a4*. Gender-specific metabolic regulation was clearly evident in female mice. *Lactococcus* and *Staphylococcus*

were positively correlated with the metabolic outcomes. In contrast, *Muribaculum* exhibited negative associations with serum glucose and lipids, as well as the *Slc2a1* and *Acat2* expressions.

3.10 Regulatory effects of FVP on gut function of mice

Functional profiling of gut microbiota was conducted using PICRUST2 based on Kyoto Encyclopedia of Genes and Genomes (KEGG) database, with key metabolic pathways differentially modulated by FVP administration (depicted in **Fig. 10)**. Compared to the SDm group, both the FMm and FHm groups exhibited significant downregulation of the steroid biosynthesis pathways (KEGG pathway ko00100), as illustrated in **Fig. 10 B** and **C**, suggesting altered cholesterol homeostasis in response to FVP intervention. An enhanced energy metabolism was evident in FVP-treated males, with FMm and FHm groups exhibited increased in the citrate cycle activity (TCA-cycle, ko00020) and glycan degradation pathways (ko00511). Notably, an improvement in protein processing within the endoplasmic reticulum (ko04141) was observed solely in FMm group, which consistent with the increased intestinal clathrin-mediated polysaccharide transport, as evidenced by the increased expression of *Clta* and *Cltc* in the large intestine of males. Dose-dependent metabolic remodeling was observed when comparing FMm and FHm groups, high-dose FVP induced pronounced upregulation of several metabolic pathways, including lipopolysaccharide biosynthesis (ko00540), sphingolipid (ko00600), biotin (ko00780), lipoic acid (ko00785), and taurine (ko00430) metabolism. Moreover, the protein digestion and absorption pathways (ko04974) showed enhancement in males treated with high-dose FVP. Gender-specific responses were evident in females, as depicted in **Fig. 10 D** and **E**, with only minor alterations detected.

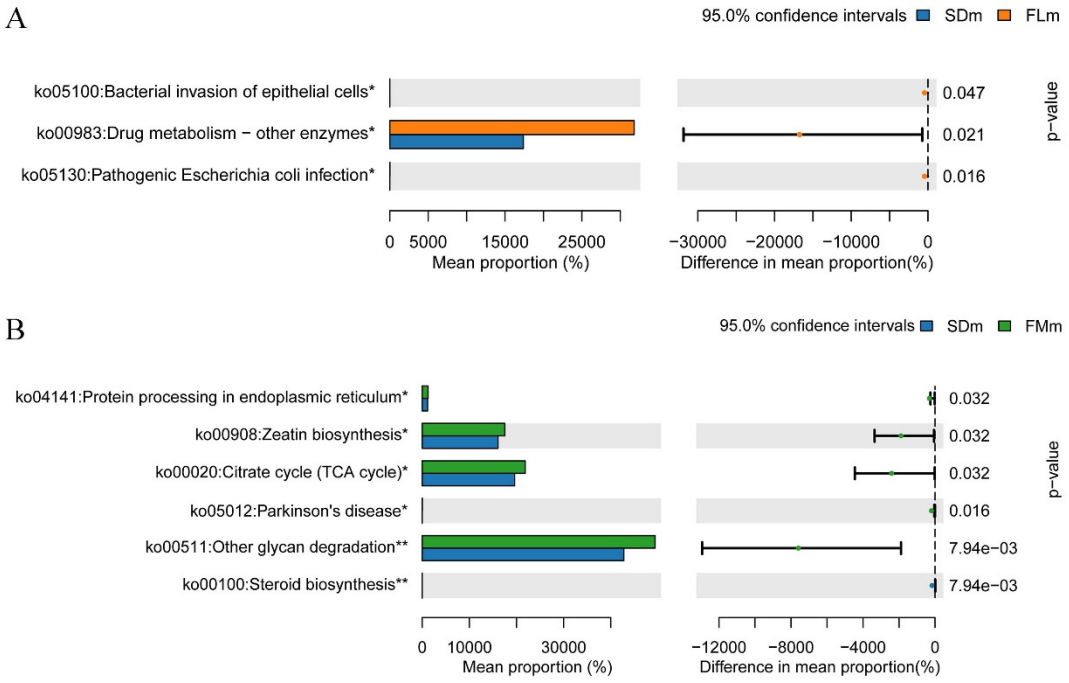

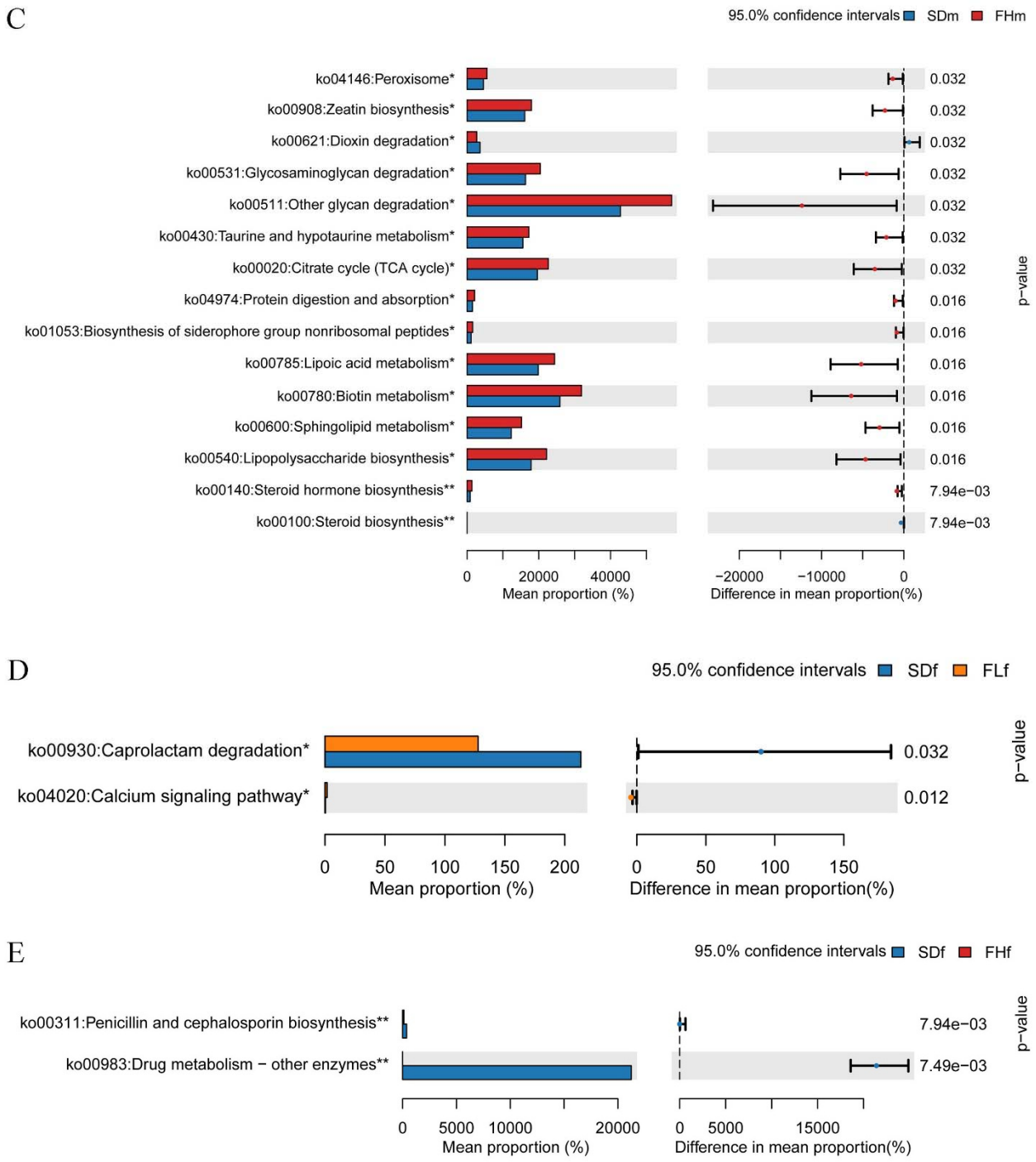

Fig. 10 PICRUSt2-predicted microbial community functional changes in (A) SDm vs FLm, (B) SDm vs FMm, (C) SDm vs FHm, (D) SDf vs FLf, (E) SDf vs FHf. Analyses were based on the database of Kyoto Encyclopedia of Genes and Genomes (KEGG), * and ** indicated significant ($P < 0.05$) and extremely significant ($P < 0.01$) of the associations.

FVP supplementation led to notable changes in the abundance of pivotal gut microbiota, specifically *P. goldsteinii* and *P. johnsonii* in males as well as *M. schaedleri*, *B. caecimuris* and *B. satroii* in females. These highlighted microbes were reported strongly correlated with alterations in glucose and lipids metabolism, as well as variations in SCFAs and bile acids levels which discussed above. Sex-stratified analysis further uncovered distinct gender-specific responses. However, these divergent patterns manifested in the changes of multiple indicators, suggested that the influence of FVP on gut microbiota and their metabolic functions might be more multifaceted than initially anticipated, thereby necessitating further investigation.

4. Conclusion

This study provides systematic evidence characterizing the transport characters and biological effects of FVP across multiple experimental models. Caco-2 cell monolayer assays demonstrated that FVP with effective intestinal absorption, further qRT-PCR analysis confirmed that clathrin-dependent endocytosis mediated FVP intestinal transport. Murine model classified FVP as a minimally toxic. Additionally, FVP treatment resulted in a reduced body weight, serum glucose and lipid levels, which attributed to the decreased gene expressions involved in glucose and lipids transporters in male and female mice intestine. Moreover, FVP supplementation led to marked changes in the abundance of pivotal gut microbiota. Collectively, these findings demonstrate that FVP exerts multifaceted functions in host metabolism through modulation of nutrient transporter expressions, and restructuring of gut microbiota-metabolite axes.

Conflict of interest

There are no conflicts of interest to declare.

Acknowledgements

This work was supported by the National Natural Science Foundation of China (No. 32302076) and the Research Foundation for Talented Scholars of Jinling Institute of Technology (jit-b-202330). Ruiqiu Zhao carried out the conducted research, statistical analysis, interpreted the data, and drafted the manuscript. Congcong Gao assisted in completing this research. Hongliang Yao, Hechao Du and Qiuhui Hu participated in the design of the study and contributed to the critical review of the paper. Liyan Zhao is the guarantor of this work and, as such, had full access to all the data in the study and takes responsibility for the integrity of the data and the accuracy of the data analysis. All authors read and approved the final manuscript.

References

[1] F.F. Anhê, A. Maretté, A microbial protein that alleviates metabolic syndrome, Nature Medicine. 23 (2017) 11-12. https://doi.org/10.1038/nm.4261.

[2] M. Barone, S. Garelli, S. Rampelli, et al., Multi-omics gut microbiome signatures in obese women: role of diet and uncontrolled eating behavior, Bmc Medicine. 20 (2022) 500. https://doi.org/10.1186/s12916-022-02689-3.

[3] C. Vals-Delgado, J.F. Alcala-Diaz, H. Molina-Abril, et al., An altered microbiota pattern precedes Type 2 diabetes mellitus development: from the CORDIOPREV study, Journal of Advanced Research. 35 (2022) 99-108. https://doi.org/10.1016/j.jare.2021.05.001.

[4] A.W.F. Janssen, T. Houben, S. Katiraei, et al., Modulation of the gut microbiota impacts nonalcoholic fatty liver disease: a potential role for bile acids, Journal of Lipid Research. 58 (2017) 1399-1416. https://doi.org/10.1194/jlr.M075713.

[5] C.A. Shively, T.C. Register, S.E. Appt, et al., Consumption of mediterranean versus western diet leads to distinct mammary gland microbiome populations, Cell Reports. 25 (2018) 47-56. https://doi.org/10.1016/j.celrep.2018.08.078.

[6] Z.P. Qu, H.B. Liu, J. Yang, et al., Selective utilization of medicinal polysaccharides by human gut *Bacteroides* and *Parabacteroides* species, Nature Communications. 16 (2025) 638. https://doi.org/10.1038/s41467-025-55845-7.

[7] R.Q. Zhao, Q.H. Hu, G.X. Ma, et al., Effects of *Flammulina velutipes* polysaccharide on immune response and intestinal microbiota in mice, Journal of Functional Foods. 56 (2019) 255-264. https://doi.org/10.1016/j.jff.2019.03.031.

[8] R.Q. Zhao, D.L. Fang, Y. Ji, et al., *In vitro* and *in vivo* functional characterization of an immune activation *Flammulina velutipes* polysaccharide based on gut microbiota regulation, Food and Agricultural Immunology. 31 (2020) 667-686. https://doi.org/10.1080/09540105.2020.1754345.

[9] R.Q. Zhao, Y. Ji, X. Chen, et al., Effects of a β-type glycosidic polysaccharide from *Flammulina velutipes* on anti-inflammation and gut microbiota modulation in colitis mice, Food & Function. 11 (2020) 4259-4274. https://doi.org/10.1039/c9fo03017d.

[10] R.Q. Zhao, Y. Ji, X. Chen, et al., Polysaccharide from *Flammulina velutipes* attenuates markers of metabolic syndrome by modulating the gut microbiota and lipid metabolism in high fat diet-fed mice, Food & Function. 12 (2021) 6964-6980. https://doi.org/10.1039/d1fo00534k.

[11] R.Q. Zhao, Y. Ji, X. Chen, et al., *Flammulina velutipes* polysaccharides regulate lipid metabolism disorders in HFD-fed mice via bile acids metabolism, International Journal of Biological Macromolecules. 253 (2023) 127308. https://doi.org/10.1016/j.ijbiomac.2023.127308.

[12] C.Y. Shi, C. Cheng, X.T. Lin, et al., *Flammulina velutipes* polysaccharide-iron(III) complex used to treat iron deficiency anemia after being absorbed via GLUT2 and SGLT1 transporters, Food Science and Human Wellness. 12 (2023) 1828-1840. https://doi.org/10.1016/j.fshw.2023.02.047.

[13] G. Iacomino, L. Di Stasio, O. Fierro, et al., Protective effects of ID331 *Triticum monococcum* gliadin on *in vitro* models of the intestinal epithelium, Food Chemistry. 212 (2016) 537-542. https://doi.org/10.1016/j.foodchem.2016.06.014.

[14] F. Li, Y.L. Wei, J. Zhao, et al., Transport mechanism and subcellular localization of a polysaccharide from *Cucurbia Moschata* across Caco-2 cells model, International Journal of Biological Macromolecules. 182 (2021) 1003-1014. https://doi.org/10.1016/j.ijbiomac.2021.04.107.

[15] Q.F. Xiang, W.J. Zhang, Q. Li, et al., Investigation of the uptake and transport of polysaccharide from Se-enriched *Grifola frondos*a in Caco-2 cells model, International Journal of Biological Macromolecules. 158 (2020) 1330-1341. https://doi.org/10.1016/j.ijbiomac.2020.04.160.

[16] P. Artursson, J. Karlsson, Correlation between oral drug absorption in humans and apparent drug permeability coefficients in human intestinal epithelial (Caco-2) cells, Biochemical & Biophysical Research Communications. 175 (1991) 880-885. https://doi.org/10.1016/0006-291X(91)91647-U.

[17] L. Feng, X. Xiao, J. Liu, et al., Immunomodulatory effects of *Lycium barbarum* polysaccharide extract and its uptake behaviors at the cellular level, Molecules. 25 (2020) 1351. https://doi.org/10.3390/molecules25061351.

[18] O.O. Ariyo, A.M. Ajayi, F.A. Attah, et al., Acute and subacute toxicological evaluation of the ethanol leaf extract of *Morus mesozygia* stapf. (Moraceae) in rodents, Journal of Ethnopharmacology. 328 (2024) 118112. https://doi.org/10.1016/j.jep.2024.118112.

[19] V. Antipova, L.M. Steinhoff, C. Holzmann, et al., Organ weights in NPC1 mutant mice partly normalized by various pharmacological treatment approaches, International Journal of Molecular Sciences. 24 (2023) 573. https://doi.org/10.3390/ijms24010573.

[20] S. Aygörmez, S. Kücükler, C. Gür, et al., Investigation of the effects of morin on potassium bromate-induced brain damage in rats via different pathways with biochemical and histopathological methods, Food and Chemical Toxicology. 201 (2025) 115466. https://doi.org/10.1016/j.fct.2025.115466.

[21] M. Song, J. Zhang, S.M. Huo, et al., Mitophagy alleviates AIF-mediated spleen apoptosis induced by AlCl3 through Parkin stabilization in mice, Food and Chemical Toxicology. 176 (2023) 113762. https://doi.org/10.1016/j.fct.2023.113762.

[22] G.E. Hurtado-Nuñez, C. Cortés-Rojo, S.G. Sánchez-Ceja, et al., Gallic, ellagic acids and their oral combined administration induce kidney, lung, and heart injury after acute exposure in Wistar rats, Food and Chemical Toxicology. 170 (2022) 113492. https://doi.org/10.1016/j.fct.2022.113492.

[23] Y.L. Ye, Y.D. Xu, J. Ji, et al., Polysaccharides extracted from *Polygonatum sibiricum* alleviate intestine-liver-kidney axis injury induced by citrinin and alcohol co-exposure in mice, Food and Chemical Toxicology. 197 (2025) 115314. https://doi.org/10.1016/j.fct.2025.115314.

[24] C. Xiao, Q.P. Wu, J.M. Zhang, et al., Antidiabetic activity of *Ganoderma lucidum* polysaccharides F31 down-regulated hepatic glucose regulatory enzymes in diabetic mice, Journal of Ethnopharmacology. 196 (2017) 47-57. https://doi.org/10.1016/j.jep.2016.11.044.

[25] X. Zong, H. Zhang, L.Y. Zhu, et al., *Auricularia auricula* polysaccharides attenuate obesity in mice through gut commensal *Papillibacter cinnamivorans*, Journal of Advanced Research. 52 (2023) 203-218. https://doi.org/10.1016/j.jare.2023.08.003.

[26] P. Lundquist, P. Artursson, Oral absorption of peptides and nanoparticles across the human intestine: opportunities, limitations and studies in human tissues, Advanced Drug Delivery Reviews. 106 (2016) 256-276. https://doi.org/10.1016/j.addr.2016.07.007.

[27] X.W. Wang, Y.H. Qiu, M.Y. Wang, et al., Endocytosis and organelle targeting of nanomedicines in cancer therapy, International Journal of Nanomedicine. 15 (2020) 9447-9467. https://doi.org/10.2147/ijn.s274289.

[28] C. Liu, Y.Q. Kou, X. Zhang, et al., Strategies and industrial perspectives to improve oral absorption of biological macromolecules, Expert Opinion on Drug Delivery. 15 (2018) 223-233. https://doi.org/10.1080/17425247.2017.1395853.

[29] J.H. Zhang, J.X. He, J.M. Huang, et al., Pharmacokinetics, absorption and transport mechanism for ginseng polysaccharides, Biomedicine & Pharmacotherapy. 162 (2023) 114610. https://doi.org/10.1016/j.biopha.2023.114610.

[30] Z.M. Zheng, X.L. Pan, H.Y. Wang, et al., Mechanism of lentinan intestinal absorption: clathrin-mediated endocytosis and macropinocytosis, Journal of Agricultural and Food Chemistry. 69 (2021) 7344-7352. https://doi.org/10.1021/acs.jafc.1c00349.

[31] M. Mueckler, B. Thorens, The SLC2 (GLUT) family of membrane transporters, Molecular aspects of medicine. 34 (2013) 121-138. https://doi.org/10.1016/j.mam.2012.07.001.

[32] R. Spiller, Inhibiting glucose absorption to treat constipation, Lancet Gastroenterology & Hepatology. 3 (2018) 588-589. https://doi.org/10.1016/s2468-1253(18)30214-0.

[33] M.Q. Hu, F. Yang, Y.W. Huang, et al., Structural insights into the mechanism of human NPC1L1-mediated cholesterol uptake, Science Advances. 7 (2021) eabg3188. https://doi.org/10.1126/sciadv.abg3188.

[34] S. Yu-Poth, D. Yin, P.M. Kris-Etherton, et al., Long-chain polyunsaturated fatty acids upregulate LDL receptor protein expression in fibroblasts and HepG2 cells, The Journal of nutrition. 135 (2005) 2541-2545. https://doi.org/10.1093/jn/135.11.2541.

[35] S. Lobo, B.M. Wiczer, A.J. Smith, et al., Fatty acid metabolism in adipocytes: functional analysis of fatty acid transport proteins 1 and 4, Journal of lipid research. 48 (2007) 609-620. https://doi.org/10.1194/jlr.M600441-JLR200.

[36] K.A. Krautkramer, J. Fan, F. Bäckhed, Gut microbial metabolites as multi-kingdom intermediates, Nature Reviews Microbiology. 19 (2021) 77-94. https://doi.org/10.1038/s41579-020-0438-4.

[37] E.A. Smith, G.T. Macfarlane, Dissimilatory amino acid metabolism in human colonic bacteria, Anaerobe. 3 (1997) 327-337. https://doi.org/10.1006/anae.1997.0121.

[38] J.M.W. Wong, R. de Souza, C.W.C. Kendall, et al., Colonic health: fermentation and short chain fatty acids, Journal of clinical gastroenterology. 40 (2006) 235-243. https://doi.org/10.1097/00004836-200603000-00015.

[39] A. Koh, F. De Vadder, P. Kovatcheva-Datchary, et al., From dietary fiber to host physiology: short-chain fatty acids as key bacterial metabolites, Cell. 165 (2016) 1332-1345. https://doi.org/10.1016/j.cell.2016.05.041.

[40] L. Li, M.L. He, H. Xiao, et al., Acetic Acid Influences BRL-3A Cell Lipid Metabolism via the AMPK Signalling Pathway, Cellular Physiology and Biochemistry. 45 (2018) 2021-2030. https://doi.org/10.1159/000487980.

[41] F. De Vadder, F. Plessier, A. Gautier-Stein, et al., Vasoactive intestinal peptide is a local mediator in a gut-brain neural axis activating intestinal gluconeogenesis, Neurogastroenterology and motility : the official journal of the European Gastrointestinal Motility Society. 27 (2015) 443-448. https://doi.org/10.1111/nmo.12508.

[42] S.C. Bridgeman, W. Northrop, P.E. Melton, et al., Butyrate generated by gut microbiota and its therapeutic role in metabolic syndrome, Pharmacological Research. 160 (2020) 105174. https://doi.org/10.1016/j.phrs.2020.105174.

[43] C.B. Newgard, J. An, J.R. Bain, et al., A branched-chain amino acid-related metabolic signature that differentiates obese and lean humans and contributes to insulin resistance, Cell metabolism. 9 (2009) 311-326. https://doi.org/10.1016/j.cmet.2009.02.002.

[44] Y.L. Cui, L.S. Zhang, X. Wang, et al., Roles of intestinal *Parabacteroides* in human health and diseases, Fems Microbiology Letters. 369 (2022) fnac072. https://doi.org/10.1093/femsle/fnac072.

[45] S.S. Qiao, C. Liu, L. Sun, et al., Gut *Parabacteroides merdae* protects against cardiovascular damage by enhancing branched-chain amino acid catabolism, Nature Metabolism. 4 (2022) 1271-1286. https://doi.org/10.1038/s42255-022-00649-y.

[46] T.R. Wu, C.S. Lin, C.J. Chang, et al., Gut commensal *Parabacteroides goldsteinii* plays a predominant role in the anti-obesity effects of polysaccharides isolated from *Hirsutella sinensis*, Gut. 68 (2019) 248-262. https://doi.org/10.1136/gutjnl-2017-315458.

[47] T. Li, N. Ding, H.Q. Guo, et al., A gut microbiota-bile acid axis promotes intestinal homeostasis upon aspirin-mediated damage, Cell Host & Microbe. 32 (2024) https://doi.org/10.1016/j.chom.2023.12.015.

[48] J. Liu, Y. Zhang, L.X. Xu, et al., *Parabacteroides johnsonii* inhibits the onset and progression of colorectal cancer by modulating the gut microbiota, Journal of Translational Medicine. 23 (2025) 734. https://doi.org/10.1186/s12967-025-06675-0.

[49] T.T. Ju, J.Y. Kong, P. Stothard, et al., Defining the role of *Parasutterella*, a previously uncharacterized member of the core gut microbiota, Isme Journal. 13 (2019) 1520-1534. https://doi.org/10.1038/s41396-019-0364-5.

[50] J.E. Bisanz, V. Upadhyay, J.A. Turnbaugh, et al., Meta-analysis reveals reproducible gut microbiome alterations in response to a high-fat diet, Cell Host & Microbe. 26 (2019) 265-272. https://doi.org/10.1016/j.chom.2019.06.013.

[51] Y. Liu, K.N. Yang, Y.Q. Jia, et al., Gut microbiome alterations in high-fat-diet-fed mice are associated with antibiotic tolerance, Nature Microbiology. 6 (2021) 874-884. https://doi.org/10.1038/s41564-021-00912-0.

[52] Z.Y. Wang, S.S. Kang, Z.H. Wu, et al., *Muribaculum* intestinale restricts *Salmonella Typhimurium* colonization by converting succinate to propionate, Isme Journal. 19 (2025) wraf069. https://doi.org/10.1093/ismejo/wraf069.

[53] X.X. Liu, Y.H. Zhang, W.H. Li, et al., Fucoidan ameliorated dextran sulfate sodium-induced ulcerative colitis by modulating gut microbiota and bile acid metabolism, Journal of Agricultural and Food Chemistry. 70 (2022) 14864-14876. https://doi.org/10.1021/acs.jafc.2c06417.

[54] S. Herp, S. Brugiroux, D. Garzetti, et al., *Mucispirillum schaedleri* antagonizes *Salmonella* virulence to protect mice against colitis, Cell Host & Microbe. 25 (2019) 681-694. https://doi.org/10.1016/j.chom.2019.03.004.

[55] R. Caruso, T. Mathes, E.C. Martens, et al., A specific gene-microbe interaction drives the development of Crohn's disease-like colitis in mice, Science Immunology. 4 (2019) eaaw4341. https://doi.org/10.1126/sciimmunol.aaw4341.

[56] Y.H. Wu, Z.Y. Liu, H.Y. Zhang, et al., Unraveling the obesity-combating potential of *Parabacteroides goldsteinii* and *Bacteroides sartorii*: a dual-probiotic approach, Probiotics and Antimicrobial Proteins. (2025) https://doi.org/10.1007/s12602-025-10537-y.

[57] P. Gu, R.J. Wei, R.F. Liu, et al., Aging-induced alternation in the gut microbiota impairs host antibacterial defense, Advanced Science. 12 (2025) https://doi.org/10.1002/advs.202411008.